3D FE dynamic modelling of offshore wind turbines in sand: natural frequency evolution in the pre– to after-storm transition

Kementzetzidis, E.; Versteijlen, Willem Geert; Nernheim, Axel; Pisano, Federico

Publication date
2018

Document Version
Final published version

Published in
9th European Conference on Numerical Methods in Geotechnical Engineering

Citation (APA)
Kementzetzidis, E., Versteijlen, W. G., Nernheim, A., & Pisano, F. (2018). 3D FE dynamic modelling of offshore wind turbines in sand: natural frequency evolution in the pre– to after-storm transition. In A. S. Cardoso, J. L. Borges, P. A. Costa, A. T. Gomes, J. C. Marques, & C. S. Vieira (Eds.), *9th European Conference on Numerical Methods in Geotechnical Engineering* (Vol. 2, pp. 1477-1484).

3D FE dynamic modelling of offshore wind turbines in sand: natural frequency evolution in the pre– to after-storm transition

Evangelos Kementzetzidis
Section of Offshore Engineering, Department of Hydraulic Engineering
Delft University of Technology, Delft, The Netherlands

Willem Geert Versteijlen
Siemens Gamesa Renewable Energy
Prinses Beatrixlaan 800, 2595 BN, Den Haag (The Netherlands)

Axel Nernheim
Siemens Gamesa Renewable Energy
Beim Strohhause 25 (BTC) 20097, Hamburg (Germany)

Federico Pisanò
Section of Geo-Engineering, Department of Geoscience and Engineering
Section of Offshore Engineering, Department of Hydraulic Engineering
Delft University of Technology, Delft, The Netherlands

ABSTRACT: 3D non-linear finite element analyses are proving increasingly beneficial to analyse the foundations of offshore wind turbines (OWTs) in combination with advanced soil modelling. For this purpose, the well-known SANISAND04 bounding surface plasticity model (Dafalias & Manzari 2004) is adopted in this work to incorporate key aspects of critical state soil mechanics into the analysis of monopile foundations in sand. The final 3D soil-foundation-OWT model is exploited to simulate the response of an 8 MW OWT to a long loading history of approximately 2 hours duration. The scope is to investigate/explain the drops in natural frequency observed in the field during storms, as well as its subsequent recovery. The numerical results point out a strong connection between transient frequency drops and pore pressure accumulation, whereas the original OWT natural frequency seems to be restored as a consequence of post-storm re-consolidation.

1 INTRODUCTION

A surge of interest on the dynamic response of OWTs has been recorded in recent years. According to van Kuik et al. 2016 improved insight from advanced 3D simulations could lead to major breakthroughs, including possible pile eigenfrequency fine tuning as a function of soil characteristics and other key variables. As dynamic-sensitive structures, OWTs and their foundations must be designed with special concern for cyclic/dynamic loading conditions.

Multiple factors may affect in reality the dynamics of an OWT during its lifetime, and particularly its first fundamental frequency f_0. Hereafter, the effects of relevant geotechnical aspects on f_0 are investigated, with focus on the operational shifts in eigenfrequency induced by (i) evolution of the pore pressure field around the monopile during loading, and (ii) changes in the local state of soil (e.g. through plastic straining and compaction/dilation) predicted via advanced constitutive modelling. Variations in soil geometry around the foundation, for instance due to scour (Germanische Lloyd 2005), are instead disregarded.

The ultimate goal of this work is to shed new light on the operational evolution of f_0 as related to fundamental hydro-mechanical processes in the soil foundation. The case of a monopile foundation founded in homogeneous medium-dense sand is explicitly considered, in the same modelling framework recently developed by Corciulo et al. 2017, Kementzetzidis et al. 2017.

2 INTEGRATED SOIL-MONOPILE-TURBINE 3D FE MODELLING

A 3D FE model of the whole sand-monopile-OWT system has been built through the OpenSees simulation platform (`http://opensees.berkeley.edu`; (McKenna 1997)). Its main modelling ingredients include (i) use of an advanced critical state, cyclic sand model, and (ii) dynamic time-domain simulation of the OWT response to an environmental loading history of remarkable duration ($\approx$ 2 hours). To accommodate the second ingredient, the trade-off between accuracy and computational burden has been resolved closer to the latter through a rather coarse FE discretisation of the 3D soil domain. This peculiar aspect of the present work is imposed by the unavoidable long duration of FE analyses aiming to examine the effect of post-storm re-consolidation. Accordingly, the main value of the results being presented lies on the qualitative side, though with the merit of highlighting fundamental aspects of OWT dynamics never tackled so far through 3D time-domain non-linear simulations.

2.1 *Hydro-mechanical FE modelling of saturated low-frequency soil dynamics*

The low-frequency dynamics of the water-saturated soil is described via the *u–p* formulation by Zienkiewicz and coworkers, based on the assumption of negligible soil-fluid relative acceleration (Zienkiewicz et al. 1999).

Spurious checkerboard pore pressure modes near the 'undrained-incompressible limit' are avoided by employing the H1-P1ssp stabilised elements proposed by (McGann et al. 2015). These 8-node equal order brick elements exploit a non-residual-based stabilisation (Huang et al. 2004) that produces an additional Laplacian term in the pore water mass balance equation. The stabilisation of the pore pressure field is controlled by a numerical parameter α to be set as suggested by (McGann et al. 2015), which can be set as a function of the average element size in the FE mesh and the elastic moduli of the soil skeleton. Importantly, two-phase ssp bricks (stabilised single-point integration hexahedra elements) also feature an enhanced assumed strain field that mitigates both volumetric and shear locking.

Time marching is performed through the well-known Newmark algorithm with parameters $\beta = 0.6$ and $\gamma = (\beta + 1/2)^2 / 4 = 0.3025$ (Hughes 1987), combined with explicit forward Euler integration of soil constitutive equations at each stress point (Sloan 1987).

It should be noted that a uniform and steady distribution of soil permeability is considered for the sake of simplicity, although in reality it may vary substantially as a function of the evolving void ratio (Shahir et al. 2012).

2.2 *SANISAND04 modelling of cyclic sand behaviour*

Modelling accurately the cyclic hydro-mechanical behaviour of sands plays a major role in the time-domain simulation of dynamic soil-foundation interaction. This study relies on the predictive capability of the SANISAND04 model by (Dafalias & Manzari 2004), available in OpenSees after the implementation developed at the University of Washington (`http://opensees.berkeley.edu/wiki/index.php/Manzari_Dafalias_Material`); (Ghofrani and Arduino 2017). While readers are referred to the relevant literature available, it is here worth recalling the main features of the SANISAND04 model:

- critical state theory included through the 'state parameter' concept proposed by (Been and Jefferies 1985, Wood et al. 1994). ;
- bounding surface formulation with kinematic/rotational hardening;
- transition from compactive to dilative response across the so-called 'phase transformation' surface, evolving in the stress-space as a function of the state parameter;
- phenomenological modelling of post-dilation fabric changes upon load reversals via a fabric-related tensor, with beneficial impact on the prediction of pore pressure build-up under undrained symmetric/two-way cyclic loading.

Despite many successful applications, the SANISAND04 model cannot predict accurately ratcheting phenomena (Niemunis et al. 2005, Corti et al. 2016), vital for a reliable prediction of monopile deformations. This limitation has been recently remedied by (Liu et al. 2017, Liu et al. 2018).

Soil parameters and soil-pile interface properties A homogenous sand deposit of Toyoura clean sand is considered, with SANISAND04 constitutive parameters listed in Table 1 after (Dafalias & Manzari 2004).

The sharp HM (Hydro-Mechanical) discontinuity at the sand-pile interface is handled by inserting a thin continuum layer of 'degraded' Toyoura sand around the monopile, both along its shaft and under the tip. The weaker interface sand features elastic shear modulus and critical stress ratio $2/3$ and $3/4$ times lower than in the intact material, respectively.

2.3 *OWT and monopile structures*

The OWT-monopile set-up assumed in this study is representative of the current industry practice and concerns a large 8 MW OWT founded in medium-dense/dense sand. Relevant structural details – courtesy of Siemens Gamesa Renewable Energy (The Hague, Netherlands) – have been all incorporated in

Table 1: Toyoura SANISAND04 parameters.

Description	Parameter	Value
Elasticity	G_0 [1]	125
	ν	0.3
Critical state	M	1.25
	c	0.712
	λ_c	0.019
	e_0	0.934
	ξ	0.7
Yielding	m	0.01
Hardening	h_0	7.05
	c_h	0.968
	n^b	1.1
Dilatancy	A_0	0.704
	n^d	3.5
Fabric	z_{max}	4
	c_z	600
Density [t/m^3]	ρ_{sat}	19.4

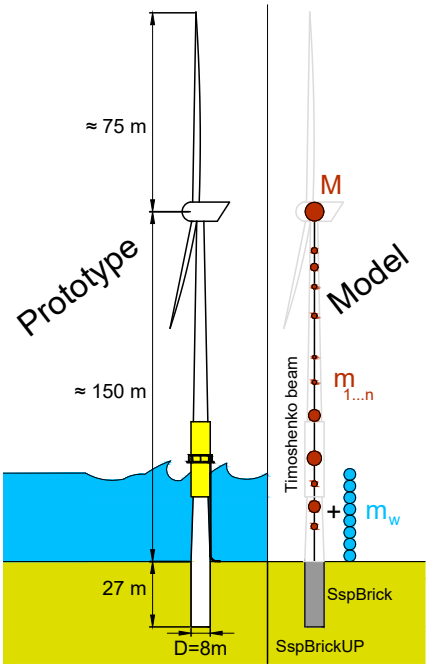

Figure 1: Idealisation and FE modelling of the OWT-foundation-soil system.

the numerical model, although incompletely reported in this paper due to confidentiality issues. In particular, the left side of Figure 1 illustrates the prototype OWT taken into account, featuring (i) a monopile with diameter $D = 8$ m, underground length $L_{pile} = 27$ m and average thickness $t = 62$ mm, (ii) a superstructure with mudline-to-hub distance of approximately 150 m, and (iii) a rotor with blade length L_{blade} in the order of 75 m. The OWT model also includes structural and equipment masses (flanges, transition piece, boat landing and working platforms, etc.), as well as the RNA lumped mass M_{RNA} (Rotor-Nacelle Assembly) at the top with suitable rotational inertia I_M associated with nacelle mass imbalances. Added mass effects due to the surrounding sea water are simplistically introduced in the form of nodal lumped masses evenly distributed along the water depth $H_w = 26$ m and calculated as twice the water mass in the submerged OWT volume (Newman 1977).

The steel structure above the mudline (wind tower and part of the monopile) is modelled as an elastic beam with variable cross-section, and subdivided into approximately 160 Timoshenko beam elements with consistent (non-diagonal) mass matrix. The underground portion of the tubular monopile is instead modelled as a 3D hollow cylinder, discretised by using 8-node, one-phase ssp bricks ($H1ssp$) (Figure 1).

A major issue in the dynamic simulation of OWTs concerns the modelling of all sources of energy dissipation (damping). In particular:

- most energy dissipation takes place within the soil domain as plastic/hysteretic damping and wave radiation away from the monopile. Absorbing viscous dampers to prevent spurious reflections are set along the lateral domain boundaries – see also (Corciulo et al. 2017);
- structural damping is introduced based on Eurocode 1 (BS EN 1991). A (Rayleigh) damping ratio $\zeta_{steel} = 0.19\%$ is assigned to all steel cross-sections at the pivot frequencies 0.1 and 80 Hz;
- hydrodynamic damping is incorporated following Leblanc and Tarp-Johansen 2010, where a damping ratio of 0.12% due to wave radiation is obtained for an OWT with $f_0 = 0.3$ Hz, pile diameter of 4.7 m and water depth at 20 m. In the lack of more specific data, a damping ratio of $\zeta_w = 0.12\%$ is assigned to the added water mass nodes (Figure 1);
- aerodynamic damping is not part of the total damping identified later in this study, although it is implicitly included in the wind loading histories applied to the OWT.

3 SENSITIVITY TO DISCRETIZATION/SIMULATION PARAMETERS

3.1 *Space/time discretisation*

Under the common assumption of mono-directional lateral loading, only half OWT has been modelled for computational convenience. The accuracy and efficiency of FE results depends strongly on space/time discretisation, i.e. on the FE mesh and time-step size adopted. As mentioned above, efficiency has been privileged here over accuracy to allow for the simulation of long time histories. The chosen domain size and mesh density are illustrated in Figure 2.

To enable 3D non-linear simulations under very long loading histories, special attention must be devoted to discretisation/simulation parameters. The

[1] Stiffness is described by the dimensionless parameter G_0 in the relevant elastic law.

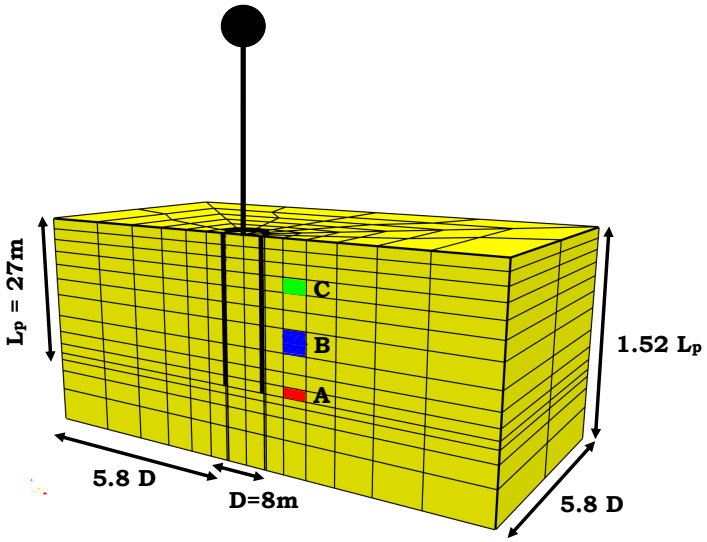

Figure 2: 3D soil mesh formed by ≈ 950 ssp bricks – A, B and C are the control points considered in the post-processing stage.

sensitivity of numerical results to the time-step size Δt has been explored along with the sensitivity of the simulated pore pressure field to the stabilisation parameter α (McGann et al. 2015). All adopted Δt values lie within the range examined in the following, whereas α has been finally set – and found satisfactory – according to the indications in McGann et al. 2015 – $\alpha = 3 \times 10^{-5}$.

3.2 *Sensitivity to time-step size*

Time-step sensitivity analyses have been performed both for short-duration (20 s – Figure 3(a), load applied at the hub) and long(er)-duration (660 s – Figure 3(b), loads applied as described later in Section 4.1) loading histories. The former has been designed to investigate the effect of a wide range of time-steps, while the latter has been devised to confirm for an 11 minutes simulations the inferences from shorter 20 s tests. It is worth noting that time integration with adaptive time-step size has been included within the global time marching scheme.

Δt values in the range $[10^{-3}; 10^{-2}]$ have been considered in short 20 s simulations, and indistinguishable results obtained at the control points A, B and C in Figure 2 – thus not reported for brevity. Then, two different Δt have been extracted from the same range and applied to the longer simulation scenario depicted in Figure 3(b). Although different by half an order of magnitude, the tested Δt values produced very similar results, for instance in terms of monopile head lateral displacement (Figure 4(a)). The impact on the computational burden of different time-step sizes is documented in Table 2, and justifies the adoption of any Δt within the range examined. As such different sections of the analysis were calculated with different Δt sizes to accommodate for the varying demand in accuracy caused by the alternating amplitude of the cyclic loads applied.

3.3 *Sensitivity to the stabilisation parameter*

The sensitivity of numerical results to the pore pressure stabilisation parameter α has been also studied over a range spanning three orders of magnitude, i.e. $\alpha = 3 \times 10^{-5}$ - $\alpha = 3 \times 10^{-8}$. The results obtained indicate a very mild influence on the global performance, for instance on the monopile deformation. It is interesting to note that choice of a specific α value also affects the computational efficiency, as shown in Table 2. In agreement with McGann et al. 2015 for the dominant element size in the FE mesh, values in the range $\alpha = 10^{-5}$ - $\alpha = 10^{-6}$ have been considered appropriate for the present application.

4 DYNAMIC OWT PERFORMANCE DURING AND AFTER A STORM

An OWT founded on a monopile embedded in dense Toyoura sand with relative density D_r=80% has been considered. In order to promote faster pore pressure dissipation, a relatively high permeability value has been set in the whole soil domain, $k = 10^{-4}$ m/s.

4.1 *Loading scenario*

This work aims to relate transient f_0 drops experienced by an OWT during storms to the evolution of the pore pressure field, including after-storm reconsolidation. In this spirit, an analysis case has been conceived to let the OWT go through different loading stages. Strong, weak loading and load removal phases to allow for consolidation are included. The overall loading scenario (sum of wind and wave loads with limited wind component due to OWT feathering) [2] is illustrated in Figure 5 and features:

1. 150 s of weak loading to estimate the 'small strain' f_0;
2. 1200 s of strong storm loading ($v_{wind} > 24m/s$) to induce transient f_0 drops;
3. 150 s of the same weak loading scenario to explore possible frequency drops caused by storm-induced, pore pressure build-up;
4. 1.7 hours (6000 s) of no loads in the domain to allow for excess pore pressure dissipation;
5. 150 s of the same weak loading scenario to observe the expected regain in f_0 due pore-pressure dissipation and void ratio variations (reconsolidation);

[2] Load time-history created by manipulating/altering load segments estimated at Siemens Gamesa Renewable Energy for an 8 MW OWT, almost fully feathered, under a strong storm. It must be noted that due to the factorisation, the loads are no more one-to-one related to the 8MW turbine.

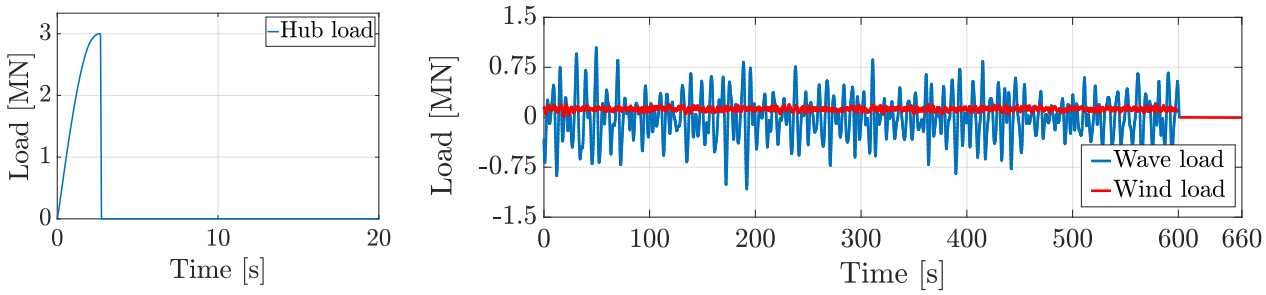

(a) (b)

Figure 3: Time-step sensitivity analysis: (a) short and (b) long loading histories.

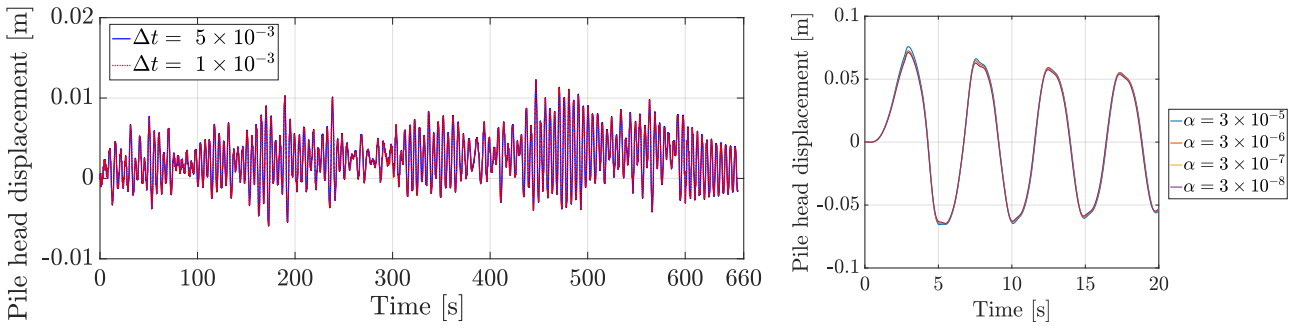

(a) Δt sensitivity (Figure 3(b) loading) (b) α sensitivity (Figure 3(a) loading)

Figure 4: Sensitivity of the monopile head lateral displacement to Δt and α.

Table 2: Explored values of time-step size and pore pressure stabilisation parameter with associated calculation time for the relevant load case. All simulations run on a i7-4790 4.00GHz CPU.

Time-step	$\Delta t = 1 \times 10^{-2}$ s	$\Delta t = 5 \times 10^{-3}$ s	$\Delta t = 1 \times 10^{-3}$ s	
Analysis time [mins]	39 mins	51 mins	215 mins	
Stabilization parameter α	$\alpha = 3 \times 10^{-5}$	$\alpha = 3 \times 10^{-6}$	$\alpha = 3 \times 10^{-7}$	$\alpha = 3 \times 10^{-8}$
Analysis time [mins]	36 mins	41 mins	47 mins	48 mins

The last 150 s of loading have been applied at excess pore pressures entirely dissipated. Therefore, any differences recorded in the response, compared to the initial 150 s of loading, should be related to previous plastic straining and changes in void ratio in the sand.

Load application The total wave force is distributed along the submerged OWT nodes, accounting for the actual wave height – nodes above the mean sea level are loaded during wave impact to ensure realistic simulation. The OWT blades are significantly pitched out under such storms, only the wind drag along the hub and tower is considered and applied to the tower bottom through a pair of equivalent point force and moment.

4.2 *Simulation results*

The evolution of the frequency content in the OWT response has been monitored by applying so-called S(Stockwell)-transformation to the simulated time history of the hub lateral displacement (Stockwell et al. 1996) – see Figure 6. As the S-transform returns the (time-varying) frequency content within a relevant band, the outcropping value associated with the maximum normalised S-amplitude at each time step has been extracted to track f_0 drops (black line in Figure 7) with respect to the fixed base natural frequency f_{FB} [3] – the same concept is also used later in Figure 8.

It is evident from Figure 6 that the natural frequency of the OWT drops during the storm, as suggested by the quadratic best-fit on the variable peak frequency extracted from the S-transform. At the

[3]The fixed base natural frequency was calculated by performing an eigenvalue analysis on the OWT fixed at the mudline.

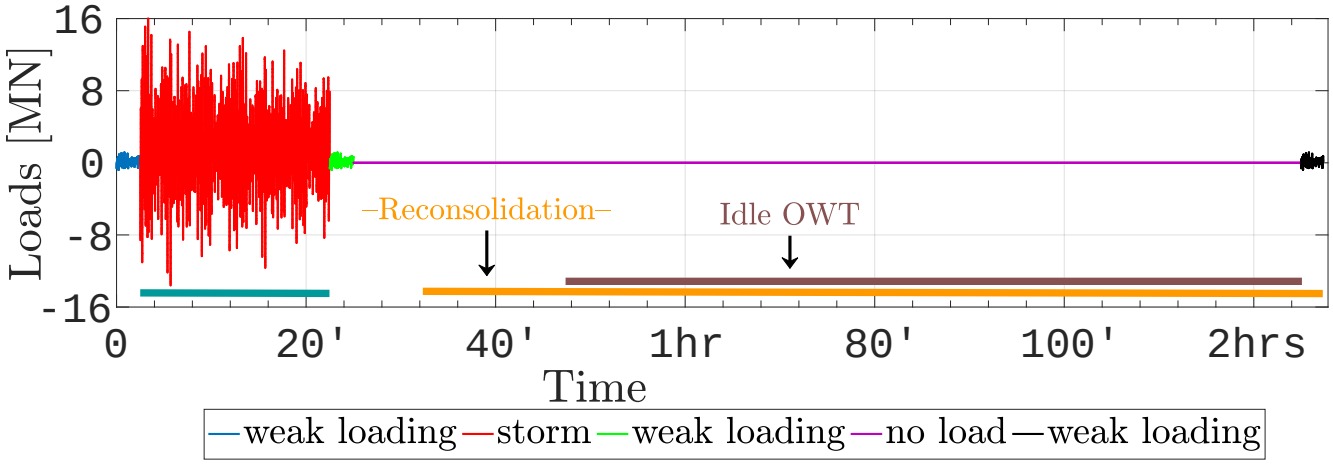

Figure 5: Assumed load time history – sum of wind and wave thrust forces.

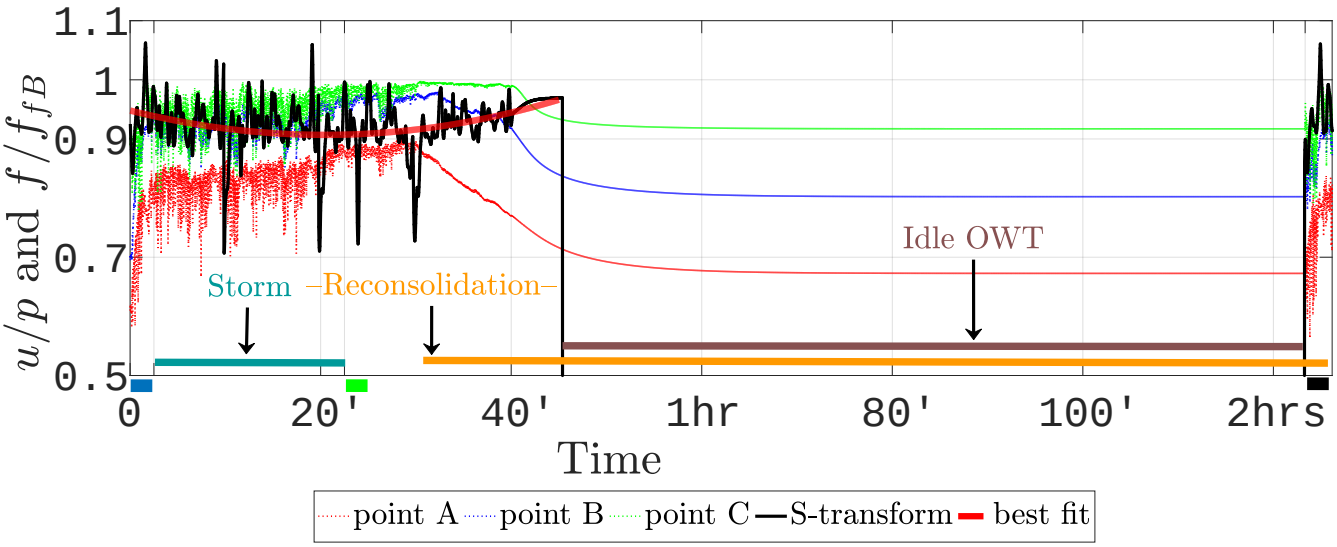

Figure 6: Thick black line: normalised OWT peak frequency; thick red line: best quadratic fit of the peak frequency time evolution; dotted lines: u/p ratios at the control points in Figure 2; thick blue, green and black lines: time range of each sub-stage in the global loading scenario in Figure 5.

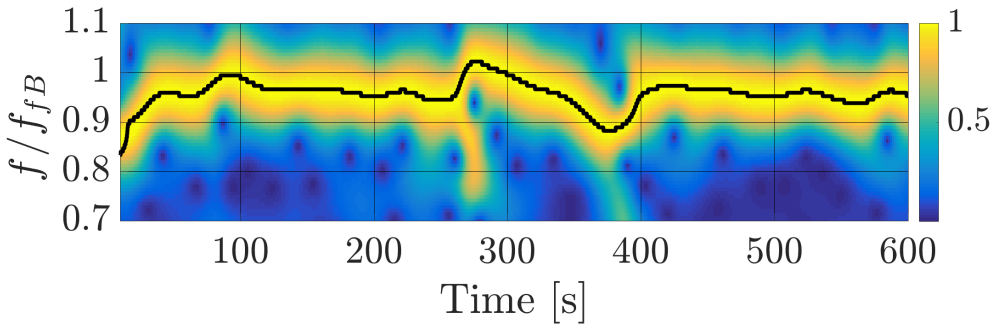

Figure 7: S-transform of the OWT response for the load time history in Figure 3(b). All frequency values are normalized with respect to the fixed-base natural frequency f_{FB} of the OWT. The colorbar indicates the magnitude of all harmonics, the thick black line underlines the evolution of the peak frequency.

same time, an increase in pore pressure – and most importantly in u/p (pore pressure-to-total mean pressure) ratio – is observed at all the control points along the embedded length of the foundation. It is comforting to observe that the local minimum of the fitting parabola lies close to onset of load removal: this evidence supports the belief that the recovery of f_0 may start right after the end of a strong loading event. A few abrupt drops of the peak response frequency are also observed, most likely due to temporary (and particularly severe) reductions in soil stiffness and, possibly, interaction with higher vibration modes.

The after-storm u/p trends in Figure 6 keep on their increasing branches even right after load removal, with further impact on the operational stiffness of the sand and cantilever-like free vibration of the OWT. The gradual decay of the free vibration amplitude allows for the dominance of the re-consolidation process, first starting at deeper soil locations (Figure 6). It can be seen that f_0 tends prominently to its pre-

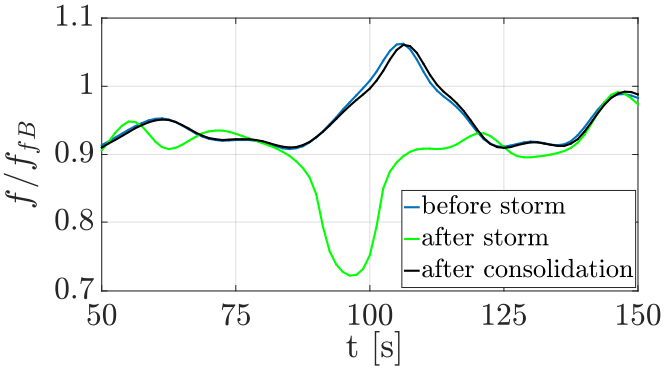

Figure 8: Time evolution of the OWT peak frequency (normalised with respect to f_{FB}) in correspondence of the three weak loading events over time (see Figures 5–6). The last 100 of the 150 seconds are displayed as the effect of the previously applied loads, for the the after storm case (green line), is significant.

storm range as re-consolidation starts occurring at the deepest control point A. It can also be observed that, as soon as the excess pore pressure at the shallowest point C is dissipated, the natural frequency of the OWT appears as fully restored. This should be attributed to the low effective confinement of shallow sand layers, more prone to pore pressure build-up and loss of shear stiffness/strength under cyclic loading. In these conditions, the upper portion of the sand deposit cannot contrast effectively the lateral loading, with immediate and apparent effect on the global foundation stiffness.

Finally, it should be noted in Figure 8 that the pre-storm and after-consolidation responses of the OWT are practically coincident. This supports the conclusion that, even during strong storm events, monopiles in (medium-dense) sand experience only temporary losses in lateral stiffness, eventually remedied by excess pore pressure dissipation and re-consolidation. However, this might not be the case, for instance, in fine-grained materials, in which cyclic loading does not only induce pore pressure build-up but also mechanical destructuration (Seidalinov and Taiebat 2014).

5 CONCLUSIONS

A long-lasting time-domain analysis including a 20 minutes storm event was performed for an 8MW OWT supported by a monopile in sand. A state-of-the-art plasticity model was employed to simulate the hydro-mechanical cyclic soil behaviour, with specific ability to describe the response of sands under a wide range of void ratio and effective confinement. A model disregarding void ratio effects would have not fully allowed to obtain the results presented in this study. Based on the evolution of the OWT dynamics from pre-storm to post-consolidation stages, it is concluded that the monopile stiffness degradation induced by even strong storm is not expected to be permanent. This inference confirms the observations from previous fields measurements, for instance from those reported by (Kallehave et al. 2015).

REFERENCES

Been, K. & M. Jefferies (1985). A state parameter for sands. *Géotechnique 35*(2), 99–112.

BS EN (1991). 1-4: 2005 eurocode 1: Actions on structures - general actions - wind actions.

Corciulo, S., O. Zanoli, & F. Pisanò (2017). Transient response of offshore wind turbines on monopiles in sand: role of cyclic hydro–mechanical soil behaviour. *Computers and Geotechnics 83*, 221–238.

Corti, R., A. Diambra, D. M. Wood, D. E. Escribano, & D. F. Nash (2016). Memory surface hardening model for granular soils under repeated loading conditions. *Journal of Engineering Mechanics*, 04016102.

Dafalias, Y. F. & M. T. Manzari (2004). Simple plasticity sand model accounting for fabric change effects. *Journal of Engineering mechanics 130*(6), 622–634.

Germanische Lloyd (2005). Guideline for the certification of offshore wind turbines.

Ghofrani, A. & P. Arduino (2017). Prediction of LEAP centrifuge test results using a pressure-dependent bounding surface constitutive model. *Soil Dynamics and Earthquake Engineering*.

Huang, M., Z. Q. Yue, L. G. Tham, & O. C. Zienkiewicz (2004, September). On the stable finite element procedures for dynamic problems of saturated porous media. *International Journal for Numerical Methods in Engineering 61*(9), 1421–1450.

Hughes, T. J. R. (1987). *The Finite Element Method: linear static and dynamic finite element analysis*. Prentice-Hall.

Kallehave, D., C. Thilsted, & A. T. Diaz (2015). Observed variations of monopile foundation stiffness. In *The 3rd Internationl symposium on Frontiers in offshore Geotechnics*, pp. 717–722. CRC Press LLC.

Kementzetzidis, E., S. Corciulo, W. G. Versteijlen, & F. Pisanò (2017). Geotechnical aspects of offshore wind turbine dynamics from 3d non-linear soil-structure simulations. *Soil Dynamics and Earthquake Engineering submitted for publication*.

Leblanc, C. & N. J. Tarp-Johansen (2010). Monopiles in sand. stiffness and damping.

Liu, H., J. A. Abell, A. Diambra, & F. Pisanò (2018). A three-surface plasticity model capturing cyclic sand ratcheting. *Géotechnique submitted for publication*.

Liu, H., F. Zygounas, A. Diambra, & F. Pisanò (2017). Enhanced plasticity modelling of high-cyclic ratcheting and pore pressure accumulation in sands. In *In Proceedings of the Xth European conference on Numerical Methods in Geotechnical Engineering (NUMGE 2017), Porto, Portugal, submitted for publication*.

McGann, C. R., P. Arduino, & P. Mackenzie-Helnwein (2015). A stabilized single-point finite element formulation for three-dimensional dynamic analysis of saturated soils. *Computers and Geotechnics 66*, 126–141.

McKenna, F. T. (1997). *Object-oriented finite element programming: frameworks for analysis, algorithms and parallel computing*. Ph. D. thesis, University of California, Berkeley.

Newman, J. N. (1977). *Marine hydrodynamics*. MIT press.

Niemunis, A., T. Wichtmann, & T. Triantafyllidis (2005). A high-cycle accumulation model for sand. *Computers and geotechnics 32*(4), 245–263.

Seidalinov, G. & M. Taiebat (2014). Bounding surface saniclay plasticity model for cyclic clay behavior. *International Journal for Numerical and Analytical Methods in Geomechanics 38*(7), 702–724.

Shahir, H., A. Pak, M. Taiebat, & B. Jeremić (2012). Evaluation of variation of permeability in liquefiable soil under earthquake loading. *Computers and Geotechnics 40*, 74–88.

Sloan, S. W. (1987). Substepping schemes for the numerical integration of elastoplastic stress–strain relations. *International Journal for Numerical Methods in Engineering 24*(5), 893–911.

Stockwell, R. G., L. Mansinha, & R. Lowe (1996). Localization of the complex spectrum: the s transform. *IEEE transactions on signal processing 44*(4), 998–1001.

van Kuik, G. A. M., J. Peinke, R. Nijssen, D. J. Lekou, J. Mann, J. N. Sørensen, C. Ferreira, J. W. van Wingerden, D. Schlipf, P. Gebraad, et al. (2016). Long-term research challenges in wind energy–a research agenda by the European Academy of Wind Energy. *Wind Energy Science 1*, 1–39.

Wood, D. M., K. Belkheir, & D. F. Liu (1994). Strain softening and state parameter for sand modelling. *Géotechnique 44*(2), 335–339.

Zienkiewicz, O. C., A. H. C. Chan, M. Pastor, B. A. Schrefler, & T. Shiomi (1999). *Computational geomechanics*. Wiley Chichester.